Computational and Theoretical Chemistry 1123 (2018) 87–95

Contents lists available at ScienceDirect

Computational and Theoretical Chemistry

journal homepage: www.elsevier.com/locate/comptc

A theoretical study of the thermal stability of the $FS(O_2)OSO_2$ radical and the recombination kinetics with the FSO_3 radical

M.P. Badenes, C.J. Cobos *, A.E. Croce

Instituto de Investigaciones Fisicoquímicas Teóricas y Aplicadas (INIFTA), Departamento de Química, Facultad de Ciencias Exactas, Universidad Nacional de La Plata, CONICET, Casilla de Correo 16, Sucursal 4, (1900) La Plata, Argentina

ARTICLE INFO

Article history:
Received 31 August 2017
Received in revised form 30 October 2017
Accepted 1 November 2017
Available online 20 November 2017

Keywords:
FSO_3
$FS(O_2)OSO_2$
$(FS(O_2)O)_2SO_2$
Quantum-chemical calculations
Transition state theory
Statistical adiabatic channel model

ABSTRACT

The kinetics of the thermal reaction of $FS(O_2)OO(O_2)SF$ with SO_2 have been theoretically studied. Experimental investigations performed at 293–323 K indicate that the FSO_3 radical, in equilibrium with the peroxide $FS(O_2)OO(O_2)SF \rightleftarrows 2\ FSO_3$ (1, -1), initially attacks the SO_2 forming the $FS(O_2)OSO_2$ radical which afterwards may dissociate back, $FSO_3 + SO_2 \rightleftarrows FS(O_2)OSO_2$ (2, -2), or recombine with FSO_3 generating the final product, $FSO_3 + FS(O_2)OSO_2 \rightarrow (FS(O_2)O)_2SO_2$ (3). Several DFT formulations and composite ab initio models were employed to characterize $FS(O_2)OSO_2$ molecular properties and to determine relevant potential energy surfaces features of reactions (2), (-2) and (3). Transition state theory calculations lead to the high pressure rate coefficients $k_{\infty,2} = 9.1 \times 10^{-14}$ exp(−5.2 kcal mol^{-1}/ RT) cm^3 molecule^{-1} s^{-1} and $k_{\infty,-2} = 4.9 \times 10^{15}$ exp(−13.9 kcal mol^{-1}/RT) s^{-1} while statistical adiabatic channel model (SACM/CT) calculations predict for the barrierless reaction (3) the expression $k_{\infty,3} = 2.9 \times 10^{-11}(T/300)^{0.4}$ cm^3 molecule^{-1} s^{-1}. The experimental phenomenological rate coefficients are very well reproduced by these rate coefficients.

1. Introduction

The knowledge of the thermal stability and the kinetics of small radicals formed from atmospheric species deserves considerable interest. In particular, a set of RSO_2 radicals are formed by association of R radicals with the important pollutant SO_2, such as HSO_2, SO_3 or $HOSO_2$. Among these, the $HOSO_2$ radical is probably the most important compound [1,2]. In addition to these termolecular processes, metastable excited adducts RSO_2^* generated by reaction of SO_2 with other atmospheric radicals such as ClO, HO_2 or NO_2, could participate as intermediates in relevant complex-forming bimolecular reactions [1,2]. The molecular properties of other SO_2-containing radicals such as FSO_2 [3–6], $ClSO_2$ [7] and CF_3OSO_2 [8] have been estimated. Species of varied stability have been postulated to participate in the reaction mechanisms, in which the fluorosulphate radical, FSO_3, is involved. In fact, the stable species $FS(O_2)ONO$ [9], $FS(O_2)ONO_2$ [10,11] and the labile complexes $FS(O_2)OOO$ [12,13], $FS(O_2)OSF_4$ [14,15] and $FS(O_2)OSO_2$ [15,16] have been reported.

The FSO_3 is an interesting radical formed by direct association of F atoms with SO_3 [17]. Under pseudo-first order conditions, the $FS(O_2)OO(O_2)SF \rightleftarrows 2\ FSO_3$ equilibrium is established [14,18–20]. This equilibrium plays a relevant role in the synthesis of numerous inorganic and organic substances realized with the peroxide $FS(O_2)OO(O_2)SF$, because the system reactivity is exclusively accounted for by the FSO_3 [21]. In addition, this system has been found particularly appropriate for studies of light-induced bistability [22], stabilization of unstable states [23] and oscillatory behavior [24].

Kinetic studies of FSO_3 reactions have received considerable attention. Pioneering kinetic and mechanistic investigations were performed by Schumacher and coworkers employing manometric methods [9–11,14–17,24–31]. More recently direct laser flash-photolysis studies have been reported [12,20,32–38]. On the other hand, early systematic spectroscopic studies of FSO_3 [39–46] have been improved by detailed infrared [47] and microwave [48] investigations.

Cady and Roberts [49] and Castellano and Schumacher [16] found that the $(FS(O_2)O)_2SO_2$ is formed as only product in the thermal reaction between $FS(O_2)OO(O_2)SF$ and SO_2. In a subsequent study, Castellano and Schumacher postulated the participation of the $FS(O_2)OSO_2$ radical to explain the $(FS(O_2)O)_2SO_2$ formation at 293–323 K [15],

$$FS(O_2)OO(O_2)SF \rightleftarrows 2FSO_3 \qquad (1,-1)$$

* Corresponding author.
E-mail address: cobos@inifta.unlp.edu.ar (C.J. Cobos).

https://doi.org/10.1016/j.comptc.2017.11.002
2210-271X/

$$FSO_3 + SO_2 \rightleftarrows FS(O_2)OSO_2 \quad (2, -2)$$

$$FSO_3 + FS(O_2)OSO_2 \rightarrow (FS(O_2)O)_2SO_2 \quad (3)$$

As aforementioned, the equilibrium constant for (1, -1), $K_{C,1}$, has been precisely determined [14,18–20]. In addition, the high pressure rate coefficients for the individual dissociation $k_{\infty,1}$ [10,33,50] and the recombination $k_{\infty,-1}$ processes have also been determined experimentally between 293 and 525 K and interpreted theoretically [20,34]. However, no studies for reactions (2), (-2) and (3) have been reported so far. Assuming that at the stationary state the equilibria (1, -1) ($K_{C,1} = k_1/k_{-1}$) and (2, -2) ($K_{C,2} = k_{-2}/k_2$) are established, the phenomenological rate coefficient $k_I = k_3 K_{C,1}/K_{C,2} = 2.1 \times 10^{-13} \exp(-15.7 \text{kcal mol}^{-1}/RT)$ cm^3 $molecule^{-1}$ s^{-1} was determined [15]. From this analysis, and assuming that reaction (3) is barrierless, a dissociation energy for the $FS(O_2)O\text{-}SO_2$ bond of 7.7 ± 1 kcal mol^{-1} was obtained [16].

The aim of the present study is to predict relevant molecular properties of $FS(O_2)OSO_2$ and to test the above reaction mechanism. For this, a large number of methods of the density functional theory (DFT) along high-level ab initio composite models were employed. Besides, rate coefficients for reaction (2), (-2) and (3) were derived using suitable reaction rate theories.

2. Computational methods

Due to the elusive nature of the exchange-correlation functional and to the difficulty to establish *a priori* the best DFT model, the following hybrid functionals were employed: B3LYP [50,51], B98 [52], B97-2 [53], mPW1PW91 [54], PBE1PBE [55], O3LYP [56], X3LYP [57], BMK [58], M05-2X [59], M06 [60], M06HF [61], M06-2X [60], mPW1LYP [54], mPW1PBE [54], mPW3PBE [54], TPSSh [62], τ-HCTHhyb [63], PBEh1PBE [64], LC-ωPBE [65], CAM-B3LYP [66], ωB97X-D [67] and HSEh1PBE [68]. All of them were combined with the Pople's 6-311++G(3df,3pd) triple split valence basis set [69]. The valence electrons of $FS(O_2)OSO_2$ were accommodated in molecular orbitals which comprise 328 basis functions based on 492 primitive Gaussians.

The correlation energy was more accurately accounted for by using ab initio multilevel models. The employed CBS-QB3 model relies on projected MP2 energies in the limit of a complete basis set [70,71]. The computed energies with the G3B3 [72] and G4 [73] model chemistries approach very well to those obtained at the QCISD(T, full)/G3Large//B3LYP/6-31G(d) and CCSD(T, full)/CBS//B3LYP/6-31G(2df,p) levels with a strong reduction in the computational resources. Besides, the G4MP2 model which uses a reduced order perturbation theory was employed in the calculations [74]. The average absolute deviations of these composite models from well-known experimental heat**s** of formation values are close to the considered chemical accuracy of ±1 kcal mol^{-1} [70–74]. An additional improvement to the predictive capability of the G3B3 method was carried out by using the bond additivity correction (BAC) procedure [75]. This empirical model applies atomic, molecular and pairwise bond corrections to the theoretical G3B3 enthalpies of formation reducing the mean absolute deviation to about 0.4 kcal mol^{-1}.

The geometries of the molecules were fully optimized using analytical gradient methods without symmetry constraints. Harmonic vibrational frequencies employed to estimate zero-point energy corrections (ZPE) were calculated with analytical second derivative methods. In all cases, real vibrational frequencies were obtained assuring that computed structures correspond to stable species. Standard enthalpies of formation (ΔH_f°) for $FS(O_2)OSO_2$ at 298 K were derived from atomization and isodesmic energies. These values, in combination with the enthalpies of formation of FSO_3 and SO_2 molecules of −120.9 [37,76] and −70.94 kcal mol^{-1} [1] were afterwards employed to calculate the $FS(O_2)O\text{-}SO_2$ bond dissociation enthalpies.

The UV/Vis absorption spectrum of $FS(O_2)OSO_2$ was predicted employing the time-dependent density functional theory (TD-DFT) [77] with the 6-311+G(3df) basis set. To cover the relevant part of the spectrum, the first fifteen electronic states of the radical were calculated.

All electronic structure calculations were performed using the Gaussian set of computer codes with default integration grids [78]. Increasing the integration grid to tight limits, such that cartesian coordinates converge to 10^{-4} Å or better, does not improve the results.

The kinetic calculations for reaction (2) were performed using the canonical version of the transition state theory (CTST) [79]. The rate coefficients for the barrierless reaction (3) were carried out with the statistical adiabatic channel model/classical trajectory (SACM/CT) formulation developed for linear rotor + linear rotor type of reactions [80,81]. For both cases, the molecular information was provided by the quantum chemical calculations. All calculations were performed within the rigid rotor/harmonic oscillator approximation.

3. Results and conclusions

3.1. Molecular conformers and harmonic vibrational frequencies of $FS(O_2)OSO_2$

The $FS(O_2)OSO_2$ radical exhibits internal rotations around the $FS(O_2)\text{-}OSO_2$ (dihedral angle FSOS) and $FS(O_2)O\text{-}SO_2$ (dihedral angle SOSO) bonds. To investigate the hindrance degree of the conformers, the corresponding electronic barriers were calculated. To this end, the total energy as a function of the dihedral angles was computed, allowing the remaining molecular structural parameters to be fully optimized. The resulting torsional potentials for the six conformers derived at the G4MP2 level of theory are depicted in Fig. 1. The $FS(O_2)\text{-}OSO_2$ potential energy curve presents a global minimum at a FSOS dihedral angle of 79.1° and a transition state for total rotation located at 5.9°. These structures are connected by an electronic barrier of 4.3 kcal mol^{-1}. On the other hand, the more stable conformer obtained from rotation around the $FS(O_2)O\text{-}SO_2$ bond lies at 174.8°. The corresponding critical configuration is located at 272° and presents a barrier height of 3.6 kcal mol^{-1}. The imaginary vibrational frequencies for these transition states

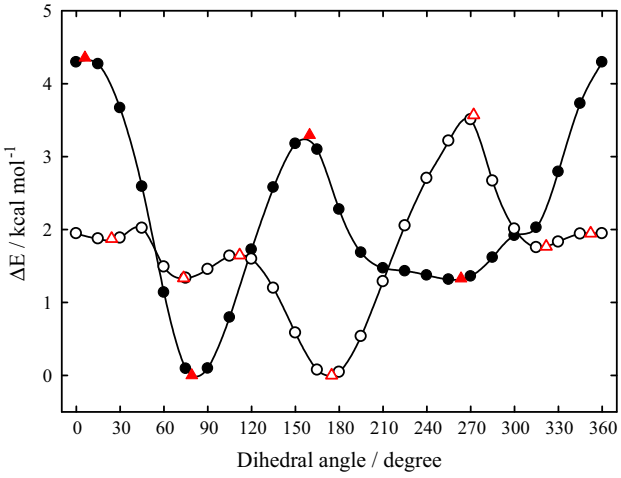

Fig. 1. Potential energy barriers for internal rotation around $FS(O_2)\text{-}OSO_2$ (●) and $FS(O_2)O\text{-}SO_2$ bonds (○) computed at the G4MP2 level. (▲) and (△) correspond to full optimized geometries at the same level.

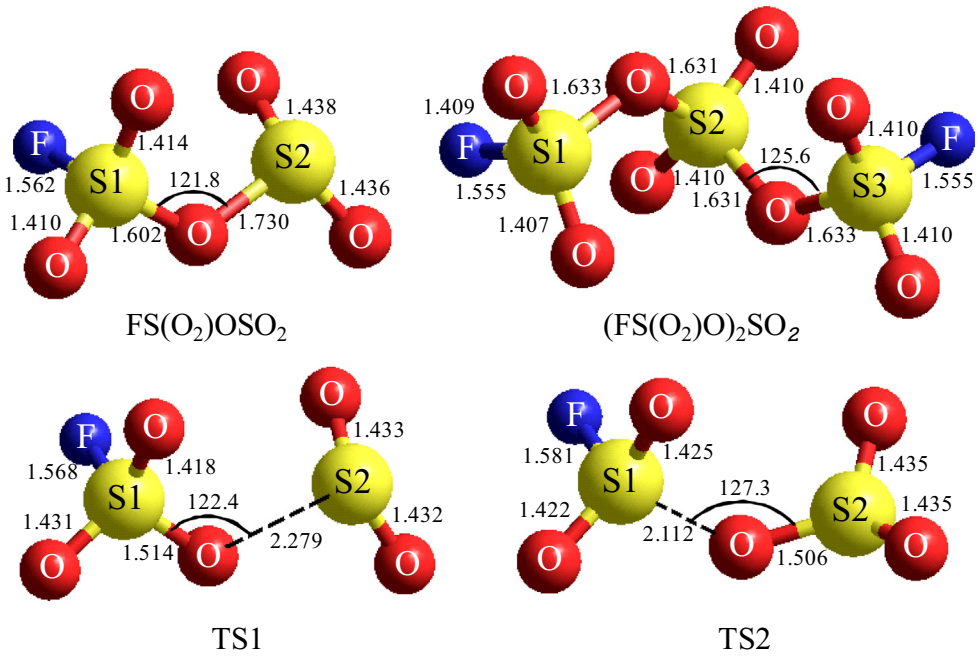

Fig. 2. Molecular structures for $FS(O_2)OSO_2$, $(FS(O_2)O)_2SO_2$ and for the TS1 and TS2 transition states optimized at the B3LYP/6-311+G(3df) level.

Table 1
Average structural parameters of $FS(O_2)OSO_2$ (bond lengths in Angstroms and angles in degrees) derived from the DFT calculations.

Parameter	Average value
r(S—F)	1.548 ± 0.005
$r(S1{=}O)_m$	1.406 ± 0.003
r(S1—O)	1.593 ± 0.004
r(S2—O)	1.701 ± 0.010
$r(S2{=}O)_m$	1.429 ± 0.003
$\angle(FS1{=}O)_m$	107.4 ± 0.1
∠(FS1—O)	98.4 ± 0.1
∠(S1OS2)	121.1 ± 0.5
∠(OS2=O)	105.1 ± 0.1
$DIH(FS1(O)_2)$	−136.2 ± 0.1
DIH(FS1OS2)	81.8 ± 0.5
DIH(S1OS2=O)	172.8 ± 0.5
$DIH(OS2(O)_2)$	132.0 ± 0.2

Table 2
Average vibrational frequencies of $FS(O_2)OSO_2$ (in cm^{-1}) derived from the DFT calculations.

Assignments	Average value	Assignments	Average value
Asym. stretch FSO_2	1520 ± 20	Bend OSO_2	509 ± 6
Asym. stretch OSO_2	1371 ± 17	Bend SO_2	486 ± 7
Sym. stretch FSO_2	1276 ± 18	Bend FS=O	435 ± 6
Sym. stretch OSO_2	1150 ± 16	Wagg FS=O	371 ± 5
Stretch SF	853 ± 16	Wagg OSO_2	292 ± 6
Stretch $FS(O_2)$—OSO_2	813 ± 18	Deformation	283 ± 6
Stretch $FS(O_2)O$—SO_2	667 ± 20	Deformation	136 ± 4
Bend FSO_2	592 ± 7	Torsion $FS(O_2)$—OSO_2	80 ± 4
Umbrella $FS(O_2)O$	546 ± 8	Torsion $FS(O_2)O$—SO_2	52 ± 3

are very low, 59 and 36 cm^{-1}. The equilibrium $FS(O_2)OSO_2$ structure is shown in Fig. 2.

Fully optimized DFT molecular structures and harmonic vibrational frequencies for the most stable $FS(O_2)OSO_2$ conformer were computed. The molecular parameters resulting from the average of all DFT calculations are listed in Table 1. Individual values are presented in Table S1 (see Supporting Information). Harmonic vibrational frequencies with their respective approximate assignments are consigned in Table S2 (see Supporting Information). The average values employed in the kinetic calculations are given in Table 2. The relatively small uncertainties in all derived properties confer reliability to the present predictions.

3.2. Thermochemistry of $FS(O_2)OSO_2$

The prediction of thermodynamic properties of molecules is a central objective of most electronic structure calculations. One of these properties is the standard enthalpy of formation, which measures the molecular stability. The value at 298 K ($\Delta H^0_{f,298}$) corresponding to $FS(O_2)OSO_2$ was determined from total atomization energies (ΣD_0) and from the isodesmic energies of the following reaction

$$FS(O_2)OSO_2 + H_2O \rightarrow HFSO_3 + HOSO_2 \quad (4)$$

ΣD_0 was calculated by subtraction of the total energy of the molecule from those of the component atoms at 0 K. Afterwards $\Delta H^0_{f,0}$ was derived by subtracting ΣD_0 from the experimental enthalpies of formation of the constituent elements. Thermal corrections are applied *a posteriori* to convert $\Delta H^0_{f,0}$ to $\Delta H^0_{f,298}$. In the second procedure, $\Delta H^0_{f,298}$ for a given molecule is obtained by combining the computed isodesmic enthalpy change with reliable enthalpies of formation of the other molecules present in the isodesmic reaction [82]. The enthalpy values of −57.798 ± 0.010 kcal mol^{-1} [1], −180 ± 2 kcal mol^{-1} [83] (for a comparison a value of −181.0 kcal mol^{-1} results from G4 calculations) and −89 ± 1.5 kcal mol^{-1} [1] were employed for H_2O, $HFSO_3$ and $HOSO_2$. The resulting $\Delta H^0_{f,298}$ values and the bond dissociation enthalpies (ΔH^0_{298}) for the $FS(O_2)OSO_2 \rightarrow FSO_3 + SO_2$ reaction, estimated using the abovementioned enthalpy of formation values for FSO_3 and SO_2, are given in Table 3. As can be seen, the DFT models lead to a large dispersion in $\Delta H^0_{f,298}$ and ΔH^0_{298} when the atomization method is employed. In fact, a value of −188.0 ± 7.4 kcal mol^{-1} was obtained for $\Delta H^0_{f,298}$, while an unrealistic value of −3.8 ± 7.4 kcal mol^{-1} was derived for ΔH^0_{298}. Thirteen DFT models led to negative ΔH^0_{298} values, while

Table 3
Calculated standard formation enthalpies for $FS(O_2)OSO_2$ and bond dissociation enthalpies for $FS(O_2)OSO_2 \rightarrow FSO_3 + SO_2$ (in kcal mol^{-1}).

Level of theory	$\Delta H^0_{f,298}$ [a]	ΔH^0_{298} [a]	$\Delta H^0_{f,298}$ [b]	ΔH^0_{298} [b]
B3LYP	−178.3	−13.5	−199.8	8.0
B98	−192.0	0.17	−199.4	7.4
B97-2	−196.7	4.9	−199.0	8.0
mPW1PW91	−181.6	−10.2	−198.6	6.8
PBE1PBE	−193.8	2.0	−198.7	6.9
O3LYP	−185.6	−6.2	−199.5	7.7
X3LYP	−177.8	−14.1	−199.7	7.9
BMK	−198.1	6.3	−198.1	6.7
M05-2X	−189.4	−2.5	−199.3	7.5
M06	−206.3	14.7	−200.1	8.3
M06HF	−159.6	−32.3	−196.6	4.8
M06-2X	−189.9	−2.0	−199.5	7.7
mPW1LYP	−160.4	−31.4	−201.9	10.1
mPW1PBE	−184.3	−7.5	−200.9	9.1
mPW3PBE	−202.5	10.7	−201.4	9.6
TPSSh	−177.1	−14.7	−200.2	8.4
τ-HCTHhyb	−205.2	13.4	−200.0	8.2
PBEh1PBE	−189.3	−2.5	−198.8	7.0
LC-ωPBE	−198.0	6.2	−197.7	5.9
CAM-B3LYP	−187.3	−4.5	−198.6	6.8
ωB97X-D	−194.0	2.1	−198.8	7.0
HSEh1PBE	−189.7	−2.1	−198.9	7.1
CBS-QB3	−198.9	7.1	−200.5	8.7
G3B3	−189.7	−2.1	−201.7	9.8
G4MP2	−201.1	9.2	−203.3	11.5
G4	−199.8	8.0	−202.7	10.9

[a] From total atomization energies.
[b] Form isodesmic energies (reaction (4)).

the B97-2, BMK, M06, mPW3PBE, τ-HCTHhyb and LC-ωPBE approaches predict values ranging from 5 to 15 kcal mol^{-1}. It is well-known that this method requires an accurate determination of the energetics of the molecule and its constituent atoms and, therefore, places a rigorous test to the quantum chemical models. It should be noted that the very low value of −2.1 kcal mol^{-1} calculated with the G3B3 model is notably increased to 6.3 kcal mol^{-1} by using the BAC-G3B3 procedure [75].

By contrast, due to the fact that the number of chemical bonds of each formal type does not change for the isodesmic reactions, systematic errors mostly attributable to both deficiencies in the treatment of the electron correlation energy and the incompleteness of the basis sets, mostly cancel [82]. As a consequence, more reliable thermodynamic values are clearly derived employing the working reaction (4). Average values of $\Delta H^0_{f,298}$ = −199.3 ± 0.7 kcal mol^{-1} and ΔH^0_{298} = 7.6 ± 0.7 kcal mol^{-1} were determined from DFT isodesmic energies. As Table 4 shows, a very good agreement with these data is obtained by using the atomization method with the CBS-Q//DFT/6-311+G(3df), G4MP2//DFT/6-311+G(3df) and G4//DFT/6-311+G(3df) composite models, which are based on optimized DFT/6-311+G(3df) structures. The average values derived from these models, respectively, for $\Delta H^0_{f,298}$ are −201.0 ± 0.3, −201.0 ± 0.2 and −200.0 ± 0.3 kcal, and for ΔH^0_{298}

Table 4
Standard formation enthalpies for $FS(O_2)OSO_2$ and bond dissociation enthalpies for $FS(O_2)OSO_2 \rightarrow FSO_3 + SO_2$ (in kcal mol^{-1}) obtained from total atomization energies.

DFT level of optimization	$\Delta H^0_{f,298}$ (CBS-Q//DFT)	ΔH^0_{298} (CBS-Q//DFT)	$\Delta H^0_{f,298}$ (G4MP2//DFT)	ΔH^0_{298} (G4MP2//DFT)	$\Delta H^0_{f,298}$ (G4//DFT)	ΔH^0_{298} (G4//DFT)
B3LYP	−201.2	9.4	−201.1	9.3	−200.0	8.2
B98	−201.4	9.6	−201.3	9.5	−200.3	8.5
B97-2	−201.2	9.4	−201.2	9.4	−200.2	8.4
mPW1PW91	−201.2	9.4	−201.1	9.3	−200.2	8.4
PBE1PBE	−201.2	9.4	−201.1	9.3	−200.3	8.5
O3LYP	−201.1	9.3	−201.1	9.3	−199.9	8.1
X3LYP	−201.3	9.5	−201.2	9.4	−200.1	8.3
BMK	−200.0	8.2	−200.1	8.3	−199.4	7.6
M05-2X	−201.0	9.2	−200.9	9.1	−200.0	8.2
M06	−200.8	9.0	−200.8	9.0	−200.0	8.2
M06HF	−199.8	8.0	−199.8	8.0	−199.2	7.4
M06-2X	−200.8	9.0	−200.7	8.9	−199.9	8.1
mPW1LYP	−201.3	9.5	−201.2	9.4	−200.2	8.4
mPW1PBE	−201.2	9.4	−201.1	9.3	−200.2	8.4
mPW3PBE	−201.4	9.6	−201.3	9.5	−200.3	8.5
TPSSh	−201.4	9.6	−201.2	9.4	−200.0	8.2
τ-HCTHhyb	−201.4	9.6	−201.3	9.5	−200.2	8.4
PBEh1PBE	−201.2	9.4	−201.2	9.4	−200.3	8.5
LC-ωPBE	−200.3	8.5	−200.4	8.6	−199.6	7.8
CAM-B3LYP	−201.0	9.2	−201.0	9.2	−200.1	8.3
ωB97X-D	−200.9	9.1	−200.9	9.1	−200.1	8.3
HSEh1PBE	−201.2	9.4	−201.2	9.4	−200.3	8.5

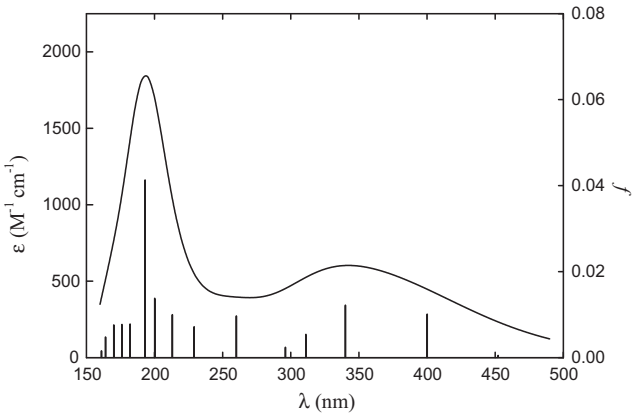

Fig. 3. UV–Vis spectrum of $FS(O_2)OSO_2$ derived from the E_m and *f* data of all TD-DFT calculations.

are 9.2 ± 0.3, 9.2 ± 0.2 and 8.2 ± 0.2 kcal mol^{-1}. Concluding, the DFT-isodesmic approach and the high-level composite models predict a value of $\Delta H^0_{f,298}$ = −200.3 kcal mol^{-1} for $FS(O_2)OSO_2$ and a FS$(O_2)O$-SO_2 bond dissociation enthalpy of 8.5 ± 1 kcal mol^{-1} which is in very good agreement with the reported one of 7.7 ± 1 kcal mol^{-1} [15]. This value is similar to the predicted for the FS(O_2)O-OO bond, ≈ 10 kcal mol^{-1} [12,13,76] but it is somewhat smaller than the estimated for CF_3O-SO_2 at the BAC-G3MP2//B3LYP/6-311+G(3df) level, 19.1 kcal mol^{-1} [8].

3.3. Absorption spectrum of $FS(O_2)OSO_2$

To compare with probable future experimental studies, the UV/Vis absorption spectrum of $FS(O_2)OSO_2$ was predicted by TD-DFT calculations [81]. This approach has emerged as the most widely-employed theoretical approach to simulate transition energies of valence excited states of molecules or open-shell species such as radicals, which can be described by combinations of single one electron transitions [84,85]. Problems related to the multi-determinantal character and spin contamination are often not important in the TD-DFT. The computed wavelengths of the band maxima (λ_m) (associated to the electronic transition energies (E_m) $\lambda_m = E_m/\hbar c$) and the oscillator strengths (*f*) for the first fifteen electronic transitions of $FS(O_2)OSO_2$ are listed in Table S3 (see Supporting Information). As before, despite the different variety of exchange and correlation functional employed, a similar trend is observed and no hybrid functional can be considered superior to the rest. Thus, the λ_m and *f* data of all of them were employed to calculate the $FS(O_2)OSO_2$ spectrum. Due to the fact that the shape of the electronic peaks with vibronic progressions normally resembles Gaussian functions, the decadic absorption coefficients (in M^{-1} cm^{-1}) were obtained by summing over all band forms, approached by $\varepsilon_{m,i} \exp[-(1/2\sigma_i^2)(E_i - E_{m,i})^2]$ functions centered at the individual $E_{m,i}$ values,

$$\varepsilon \cong \sum_i \varepsilon_{m,i} \exp\left[-\left(\frac{1}{2\sigma_i^2}\right)(E_i - E_{m,i})^2\right] \quad (5)$$

Here $\varepsilon_{m,i} = 1.15 \times 10^4 (f_i/\sigma_i)$ are suitable weight factors for each electronic transition. For the full width of the band at 1/e, a standard value of σ = 0.4 eV was assumed for all transitions. The simulated UV–Vis spectrum shown in Fig. 3, exhibits a strong band located at about 195 nm (ε ≈ 1840 M^{-1} cm^{-1}) and a broad absorption band at about 345 nm (ε ≈ 600 M^{-1} cm^{-1}). It is interesting to note that the first band lies in the wavelengths region where the SO_2 exhibits a strong absorption, near 200 nm [86], while the second one resembles the band observed near 360 nm for the weakly bonded $FS(O_2)OOO$ radical isolated a 6 K in an Ne matrix [13].

3.4. Kinetics of the formation and decomposition of $FS(O_2)OSO_2$

$(FS(O_2)O)_2SO_2$ is the only product formed in the thermal reaction between $FS(O_2)OO(O_2)SF$ and SO_2 [49]. At 293–323 K this is a homogeneous reaction, independent of the total pressure (8–60 Torr $FS(O_2)OO(O_2)SF$ and 10–100 Torr SO_2) and of the presence of O_2 [16]. The rates of the $FS(O_2)OO(O_2)SF$ and SO_2 consumption and of the $(FS(O_2)O)_2SO_2$ formation are directly proportional to the reagents concentrations: $-d[FS(O_2)OO(O_2)SF]/dt = -d[SO_2]/dt = d[(FS(O_2)O)_2SO_2]/dt = k_I[FS(O_2)OO(O_2)SF][SO_2]$. This was initially interpreted assuming that the reaction proceeds through either a single reaction step $FS(O_2)OO(O_2)SF + SO_2 \rightarrow (FS(O_2)O)_2SO_2$, or following the successive processes $FS(O_2)OO(O_2)SF + SO_2 \rightarrow FS(O_2)OSO_2 + FSO_3$ and $FS(O_2)OSO_2 + FSO_3 \rightarrow (FS(O_2)O)_2SO_2$ [16]. A more plausible explanation was proposed a few years later by Castellano and Schumacher [15]. They postulated that the reaction mechanism is initiated by the attack of the FSO_3 radical (present in the $FS(O_2)OO(O_2)SF \rightleftarrows 2\ FSO_3$ equilibrium) to SO_2. Afterwards, the generated $FS(O_2)OSO_2$ radical either dissociates backwards to the reagents or reacts with FSO_3 forming the very stable product $(FS(O_2)O)_2SO_2$ [16,79]. Therefore, the mechanism which allows to interpret all of the experimental observations is formed by reactions (1, -1), (2, -2) and (3). If the equilibrium (2, -2) is not established at the stationary state, the consumption and formation rates are proportional to $[FS(O_2)OO(O_2)SF]^{1/2}[SO_2]$, against the experimental reaction rate equation. The postulated mechanism leads to the global rate coefficient $k_I = k_3 K_{C,1}/K_{C,2} = 2.1 \times 10^{-13} \exp(-15.7\ kcal\ mol^{-1}/RT)\ cm^3\ molecule^{-1}\ s^{-1}$ [15]. With the aim of testing this mechanism and to obtain the complete kinetic information of the system, a theoretical study of the elementary processes (2), (-2) and (3) was carried out.

3.4.1. Equilibrium constants for $FS(O_2)OO(O_2)SF \rightleftarrows 2\ FSO_3$ and $FSO_3 + SO_2 \rightleftarrows FS(O_2)OSO_2$

The equilibrium (1, -1) has been the subject of several experimental studies [14,18–20]. We used here the equilibrium constant values derived at 321–381 K from direct laser flash photolysis determinations of $k_{\infty,1}$ and $k_{\infty,-1}$ (Eq. (6)) [20], which are in very good agreement with those obtained previously at higher temperatures (see Fig. S1 of Supporting Information) [14,18,19],

$$K_{C,1} = 1.45 \times 10^{27} \exp(-21.3 \pm 0.8\ kcal\ mol^{-1}/RT)\ molecule\ cm^{-3} \quad (6)$$

Reported standard reaction enthalpy and entropy (ΔS^0_{298}) changes at 298 K are listed in Table S4 (see Supporting Information).

To calculate $K_{C,2}$, the average of $FS(O_2)OSO_2$ vibrational frequencies given in Table 1 and the average rotational constants derived from the individual DFT molecular structures: A = 0.114 ± 0.001, B = 0.036 ± 0.003 and C = 0.033 ± 0.003 cm^{-1} were employed. The FS(O_2)O-SO_2 and FS(O_2)-OSO_2 torsional motions with frequencies of 52 and 80 cm^{-1}, barriers heights of 3.6 and 4.3 kcal mol^{-1} and reduced moments of inertia of 37.0 and 66.2 amu $Å^2$ were considered as hindered internal rotors. The corresponding partition functions were estimated using the Troe's approach of Ref. [87]. Experimental vibrational frequencies for FSO_3 (161.6 (2), 426.2 (2), 531.0, 832.6, 931.5 (2) and 1052.4 cm^{-1} [47]) and SO_2 (517.69, 1151.38 and 1361.76 cm^{-1} [88]) were employed. In addition, rotational constants for FSO_3 (0.173, 0.173 [48] and 0.181 cm^{-1} from B3LYP/6-311+G(3df) calculations) and for SO_2 (2.028, 0.344 and 0.294 cm^{-1} [89]) were used. The value ΔH^0_0 = 7.9 ± 0.6

kcal mol^{-1} obtained from CBS-QB3//B3LYP/6-311+G(3df), G3//B3LYP/6-311+G(3df) and G4//B3LYP/6-311+G(3df) atomization values at 298 K (Table 4) was employed for the enthalpy change at 0 K. The resulting $K_{C,2}$ values are very well reproduced by the following expression

$$K_{C,2} = 5.4 \times 10^{28} \exp(-8.7 \text{ kcal mol}^{-1}/RT) \text{ molecule cm}^{-3} \quad (7)$$

The standard reaction enthalpy and entropy changes derived from the temperature dependence of $K_{p,C,2} = K_{C,2}(RT)$ over the 293–323 K range are respectively 9.3 kcal mol^{-1} and 44.8 cal mol^{-1} K^{-1}.

3.4.2. High pressure rate coefficients for $FSO_3 + FS(O_2)OSO_2 \rightarrow (FS(O_2)O)_2SO_2$

To estimate the phenomenological rate coefficient $k_I = k_3 K_{C,1}/K_{C,2}$ to compare with the experimental one, the knowledge of k_3 is required. This is a single bond formation reaction between two radicals for which no activation barrier was found. At the total pressures of Ref. [16], the system is surely very close to the high pressure regime and can be interpreted by the SACM/CT formulation development for two interacting linear rotors [80,81]. This model is based on a Morse potential for the formed bond $V = D_e [1 - \exp(-\beta(r - r_e))]^2$ where D_e is the bond dissociation energy and r_e is the distance between the center of mass of the two combining species. The range parameter β determines the isotropy of the potential energy surface. The evolution of the transitional modes $\nu(r)$ along the minimum energy path (the anisotropic potential) is modelled by $\nu(r) = \nu(r_e) \exp[-\alpha(r - r_e)]$ functions, being α the so-called losseness parameter [90].

The limiting high pressure rate coefficients can be factorized as follow: $k_\infty = k_\infty^{PST} f_{rigid}$ [91]. Here k_∞^{PST} is the high pressure rate coefficient at the phase space limit, which determinates the upper bound of k_∞. The rigidity factor f_{rigid} accounts for the contributions of the degrees of freedom orthogonal to the reaction coordinate, i.e. the transitional modes. In the frame of the SACM/CT, k_∞^{PST} is given by

$$k_\infty^{PST} = f_{sim} f_{el} \frac{(8 \pi k T/\mu)^{1/2}}{\beta^2} (31.153 - 18.158 X + 0.8685 X^2) \quad (8)$$

where $X = \ln(kT/D_e) - \beta r_e + 4$. For the present case, the stoichiometric coefficient f_{sim} is 1, the electronic degeneracy factor f_{el} is 0.25, the collisional reduced mass μ is 10.7 g mol^{-1}, r_e = 3.4 Å and D_e = 77.3 kcal mol^{-1} (derived, after B3LYP/6-311+G(3df) zero-point energy corrections (see Table S5 of Supporting Information), from the value $\Delta H^0_{f,298}$ = −395.0 kcal mol^{-1} obtained at the G4MP2 level for $(FS(O_2)O)_2SO_2$ from the isodesmic reaction $(FS(O_2)O)_2SO_2 + 2\,H_2O \rightarrow 2\,HFSO_3 + HOSO_2$). The Morse parameter $\beta = (F_{O-S}/2D_e)^{1/2} = 2.38$ Å^{-1} was estimated from the $FS(O_2)O\text{-}SO_2$ stretching force constant of F_{O-S} = 6.10 mdyn Å^{-1}. As Table 5 shows, the resulting $k_{\infty,3}^{PST}$ values obtained at the experimental temperatures of 293, 303 and 323 K [15,16] are close to 2.8×10^{-10} cm^3 molecule^{-1} s^{-1}.

The rigidity factor is approached as

$$f_{rigid} = \left\{1 - 2.31 C_{eff} (\beta r_e)^{1/2} \exp\left[\frac{(X-4)}{2.044}\right]\right\} (1 + 0.75 Z + Z^4)^{-1/4} \quad (9)$$

where $Z = (d C_{eff})^n$ with $C_{eff} = [1 + 0.42(2\alpha/\beta - 1) + (2\alpha/\beta - 1)^2]\{2\varepsilon_t^2\varepsilon_s^2\varepsilon_a^2/[B_1B_2(B_1 + B_2)]\}^{1/3}/2D_e$. Here, ε_t, ε_s and ε_a are the vibrational frequencies for the torsion, symmetrical and asymmetrical deformations modes of the formed molecule, while B_1 and B_2 are the reagents rotational constants. The parameter n depends on the angle θ formed between both rotor axes and molecular axis: $n = 1 - 0.5\sin^2\theta + \sin^4\theta$, while d is a complex function of ε_t, ε_s, ε_a and θ.

In the SACM/CT calculations of reaction (3), the following molecular data (in cm^{-1}) where used: ε_t = 104, ε_s = 138, ε_a = 137, B_1 = 0.173 and B_2 = 0.0338. The last two values correspond, respectively, to the average of the smallest rotational constants of FSO_3 and $FS(O_2)OSO_2$ radicals. For θ a value of 76° was employed. As aforementioned, the anisotropic part of the potential is accounted for by the α parameters. In contrast to other reactions in which α has been obtained from quantum-chemical calculations [92–94], the large mixture of vibrational modes in $(FS(O_2)O)_2SO_2$ precludes a similar determination of the transitional modes evolution along the MEP. As a consequence, the standard value $\alpha = (0.5 \pm 0.1)$ β Å^{-1} was employed here [91]. This value has been found to reproduce satisfactorily the SACM rate coefficients of a large number of recombination/dissociation reactions. The resulting f_{rigid} and $k_{\infty,3}$ values are listed in Table 5. They can be very well fitted with the expression

$$k_{\infty,3} = 2.9 \times 10^{-11} \left(\frac{T}{300}\right)^{0.4} \text{ cm}^3 \text{ molecule}^{-1} \text{ s}^{-1} \quad (10)$$

These values are close to the measured at 298 K for the related radical - radical reaction $FSO_2 + FSO_3 \rightarrow FS(O_2)O(O_2)SF$ of 6.5×10^{-11} cm^3 molecule^{-1} s^{-1} [37] for which a reaction enthalpy of −75.0 kcal mol^{-1} was estimated at the G3MP2B3 level. By contrast, a much smaller high pressure rate coefficient of 4.5×10^{-14} cm^3 molecule^{-1} s^{-1} has been experimentally determined for reaction (-1) at room temperature (reaction enthalpy of −22.1 kcal mol^{-1}) [20].

Table 5
$k_{\infty,3}^{PST}$, $k_{\infty,3}$ (in cm^3 molecule^{-1} s^{-1}) and $f_{rigid,3}$ values computed with the SACM/CT.

T (K)	$k_{\infty,3}^{PST}$	$f_{rigid,3}$	$k_{\infty,3}$
293	2.79×10^{-10}	0.105	2.92×10^{-11}
303	2.82×10^{-10}	0.105	2.96×10^{-11}
323	2.89×10^{-10}	0.105	3.03×10^{-11}

3.4.3. High pressure rate coefficients for $FSO_3 + SO_2 \rightarrow FS(O_2)OSO_2$

Appears interesting at this time to predict the rate coefficient for reaction (2) at the high pressure limit. As the calculations of the electronic potential along MEP show, by contrast to reactions (-1) and (3), this process exhibits a small electronic barrier. The molecular structures of the involved transition states, $FS(O_2)O\text{---}SO_2^\#$ (TS1) and $FS(O_2)\text{---}OSO_2^\#$ (TS2), are shown in Fig. 1. The energetics for both reactions are listed in Table 6 and Fig. 4. The high electronic barrier computed for the $FSO_3 + SO_2 \rightarrow FSO_2 + SO_3$ reaction indicates that this is an extremely slow process. Therefore, it does not play any role in the present mechanism.

As observed in Table 6, the G4 energies are quite sensitive to the $FS(O_2)O\text{---}SO_2^\#$ molecular structures. In fact, using B3LYP/6-311+G(3df) geometries instead of the original ones, B3LYP/6-31G(2df,p), a significant larger activation enthalpy is recovered. However, only minor differences are observed by employing the CBS-QB3 (structures based on B3LYP/6-311G(2d,d,p) calculations) and G3B3 (structures based on B3LYP/6-31G(d) calculations) models. The average value of 5.0 kcal mol^{-1} obtained from the CBS-QB3//B3LYP/6-311+G(3df), G3//B3LYP/6-311+G(3df) and G4//B3LYP/6-311+G(3df) results was selected to estimate the CTST rate coefficient of reaction (2). For this, the above FSO_3 and SO_2 molecular parameters, the B3LYP/6-311+G(3df) vibrational frequencies for $FS(O_2)O\text{---}SO_2^\#$ of 137i, 25, 57, 82, 147, 207, 368, 369, 481, 499, 509, 532, 779, 855, 1154, 1168, 1351 and 1371 cm^{-1} and the TS1 rotational constants values of 0.110, 0.0286 and 0.0267 cm^{-1} were used. The vibrational mode associated to the $O\text{-}SO_2$ moiety (25 cm^{-1}) was considered as a free rotor with a reduced moment of

Table 6
Reaction and activation enthalpies (in kcal mol^{-1}) for reactions $FSO_3 + SO_2 \rightarrow FS(O_2)OSO_2$ and $FS(O_2)OSO_2 \rightarrow FSO_2 + SO_3$.

Level of theory	$FSO_3 + SO_2 \rightarrow FS(O_2)OSO_2$		$FS(O_2)OSO_2 \rightarrow FSO_2+SO_3$	
	ΔH_0^0	$\Delta H_0^{\#}$ (TS1)	ΔH_0^0	$\Delta H_0^{\#}$ (TS2)
CBS-QB3	−8.0	6.4	11.3	29.8
G3B3	−7.2	5.3	11.2	29.9
G4MP2	−10.9	0.55	13.8	32.6
G4	−9.9	1.9	13.8	31.9
CBS-Q//B3LYP/6-311+G(3df)	−9.1	6.1	12.1	31.0
G3//B3LYP/6-311+G(3df)	−8.5	4.7	12.1	30.7
G4MP2//B3LYP/6-311+G(3df)	−11.1	3.4	13.8	32.6
G4//B3LYP/6-311+G(3df)	−10.1	4.1	13.9	31.9

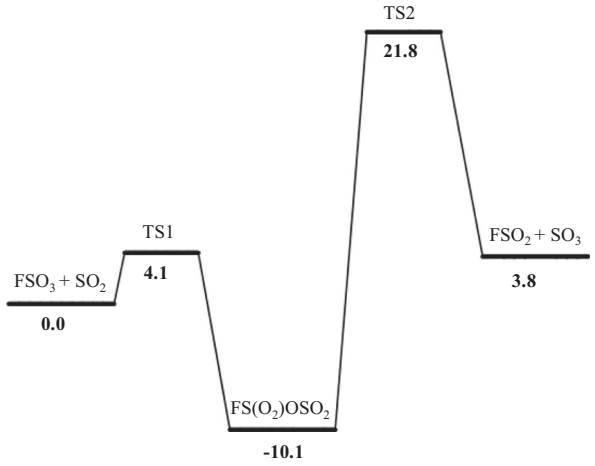

Fig. 4. Schematic diagram of the potential energy surface (in kcal mol^{-1}) of the reaction between FSO_3 and SO_2 at the G4//B3LYP/6-311+G(3df) level.

inertia of 35.3 amu Å^2. The resulting rate coefficients for reaction (2) at 293–323 K are very well represented by the expression

$$k_{\infty,2} = 9.1 \times 10^{-14} \exp(-5.2 \text{ kcal mol}^{-1}/RT) \text{ cm}^3 \text{ molecule}^{-1} \text{ s}^{-1} \quad (11)$$

Although reaction (2) exhibits small rate coefficients, the large SO_2 concentration employed (10–100 Torr) in Ref. [16] leads to the rapid establishment of equilibrium (2, -2).

The Arrhenius equation derived for $k_{\infty,-2}$ from Eqs. (6) and (7)

$$k_{\infty,-2} = 4.9 \times 10^{15} \exp(-13.9 \text{ kcal mol}^{-1}/RT) \text{ s}^{-1} \quad (12)$$

exhibits a normal preexponential factor.

3.4.4. Phenomenological rate coefficient k_I

A comparison between the experimental and calculated k_I values is presented in this last section. The relevant equilibrium constants and rate coefficients required to evaluate $k_I = k_3 K_{C,1}/K_{C,2}$ are given in Table 7. The experimental values were obtained from the equation

Table 7
Comparison between experimental and calculated k_I values. $K_{C,1}$ and $K_{C,2}$ in molecule cm^{-3}, $k_{\infty,3}$ and k_I in cm^3 molecule^{-1} s^{-1}.

T (K)	$K_{C,1}$	$K_{C,2}$	k_3	k_I[a]	k_I[b]
293	1.9×10^{11}	1.8×10^{22}	2.9×10^{-11}	3.1×10^{-22}	3.9×10^{-22}
303	6.3×10^{11}	2.9×10^{22}	3.0×10^{-11}	6.5×10^{-22}	9.6×10^{-22}
323	5.6×10^{12}	7.0×10^{22}	3.0×10^{-11}	2.4×10^{-21}	4.8×10^{-21}

[a] Calculated.
[b] Experimental.

$k_I = 2.1 \times 10^{-13} \exp(-15.7 \text{ kcal mol}^{-1}/RT) \text{ cm}^3 \text{ molecule}^{-1} \text{ s}^{-1}$. As observed, the theoretical values are a factor of ≈1.3–2.0 smaller than the experimental ones. These differences can be reconciled by reducing the employed $\Delta H_0^0 = 7.9 \pm 0.6$ kcal mol^{-1} for the equilibrium (2, -2) in only ≈0.2–0.4 kcal mol^{-1}. Besides, it should be noted that an uncertainty of about a factor of two in k_3 may be expected on the basis of the potential energy surface uncertainty ($\alpha = (0.5 \pm 0.1)$ βÅ^{-1}). Taking into account the inherent experimental and theoretical uncertainties, the agreement between the experimental and theoretical k_I values is certainly very good.

4. Conclusions

A quantum chemical and theoretical kinetic study of the thermal reaction between $FS(O_2)OO(O_2)SF$ and SO_2 over the 293–323 K range was carried out. Previous investigations show that the mechanism formed by two equilibria (reactions (1, -1) and (2, -2)) and reaction (3) explain all of the experimental data [15]. Theoretical calculations performed with twenty-two hybrid functionals and the CBS-QB3, G3B3, BAC-G3B3, G4MP2 and G4 model chemistries allowed to characterize the relevant structural, spectroscopic and thermodynamic properties of the $FS(O_2)OSO_2$ radical. The enthalpy dissociation obtained at 0 K for the $FS(O_2)O{-}SO_2$ bond of 8.5 ± 1 kcal mol^{-1} agrees very well the experimental value of 7.7 ± 1 kcal mol^{-1} [15]. Rate coefficients values of $k_{\infty,2} = 9.1 \times 10^{-14} \exp(-5.2\text{kcal mol}^{-1}/RT)$ cm^3 molecule^{-1} s^{-1}, $k_{\infty,-2} = 4.9 \times 10^{15} \exp(-13.9 \text{ kcal mol}^{-1}/RT)$ s^{-1} and $k_{\infty,3} = 2.9 \times 10^{-11}(T/300)^{0.4}$ cm^3 molecule^{-1} s^{-1} were calculated. Employing these rate coefficients and those experimentally measured for the equilibrium (1, -1) [20], phenomenological rate coefficients only about a factor of two smaller than those experimentally determined were obtained, confirming the mechanism early proposed by Castellano and Schumacher, our unforgettable mentors.

Acknowledgements

This research project was supported by the Universidad Nacional de La Plata (11/X676), the Consejo Nacional de Investigaciones Científicas y Técnicas CONICET (PIP 2012-1134 and PIP 2012-0134) and the Agencia Nacional de Promoción Científica y Tecnológica (PICT 2012-0478).

Appendix A. Supplementary material

Supplementary data associated with this article can be found, in the online version, at https://doi.org/10.1016/j.comptc.2017.11.002.

References

[1] S.P. Sander, R.R. Friedl, J.R. Barker, D.M. Golden, M.J. Kurylo, P.H. Wine, J.P.D. Abbatt, J.B. Burkholder, C.E. Kolb, G.K. Moortgat, R.E. Huie, V.L. Orkin, Chemical Kinetics and Photochemical Data for Use in Atmospheric Studies, NASA/JPL Data Evaluation, JPL Publication 06-2 Evaluation No. 17, NASA, Pasadena, CA, June 1, 2011. http://jpldataeval.jpl.nasa.gov.
[2] R. Atkinson, D.L. Baulch, R.A. Cox, J.N. Crowley, R.F. Hampson, R.G. Hynes, M.E. Jenkin, M.J. Rossi, J. Troe, Evaluated kinetic and photochemical data for atmospheric chemistry: Volume I - gas phase reactions of O_x, HO_x, NO_x and SO_x species, Atmos. Chem. Phys. 4 (1461–1738) (2004), https://doi.org/10.5194/acp-4-1461-2004.
[3] Z. Li, Ab initio study on the dissociation pathways of XSO_2 (X = Cl, F) radicals, Chem. Phys. Lett. 269 (1997) 128–137.
[4] Z. Li, Ab Initio Study of the Electronic Structure of XSO and XSO_2 (X = F, Cl) Radicals, J. Phys. Chem. A. 101 (1997) 9545–9550.
[5] M.E. Tucceri, M.P. Badenes, C.J. Cobos, Theoretical study of the heats of formation of SF, FSO, FSO_2 and HSO radicals, Z. Physik. Chem. 214 (2000) 1193–1208.

[6] A.F. Khalizov, P.A. Ariya, Stability of XSO_2 (X=F, Cl, and Br) radical: impact of the basis set on X-S bonding energy in ab initio and DFT calculations, Chem. Phys. Lett. 350 (2001) 173–180.

[7] M. Bahou, S.-F. Chen, Y.-P. Lee, Production and infrared absorption spectrum of $ClSO_2$ in matrices, J. Phys. Chem. A 104 (2000) 3613–3619.

[8] C.J. Cobos, A.E. Croce, Theoretical study of the absorption spectrum and the thermochemistry of the CF3OSO3 radical, Z. Naturforsch. 65a (2010) 720–724.

[9] G. von Ellenrieder, H.J. Schumacher, Der Mechanismus der thermischen Reaktion zwischen Bis-Fluorsulfurylperoxid und Stickstoffmonoxid, Z. Physik. Chem. 59 (1968) 151–156.

[10] G. von Ellenrieder, H.J. Schumacher, Die Kinetik der thermischen Reaktion zwischen Bis-Fluorsulfurylperoxid und Stickstoffdioxid, Z. Physik. Chem. 59 (1968) 157–165.

[11] G. von Ellenrieder, H.J. Schumacher, Die Kinetik der thermischen Reaktion zwischen Fluorfluorsulfonat (F_2SO_3) und Stickstoffdioxid, Z. Physik. Chem. 62 (1968) 159–167.

[12] A.E. Croce, C.J. Cobos, E. Castellano, Kinetics of formation and unimolecular decomposition of the $FS(O_2)OOO$ radical, J. Fluor. Chem. 82 (1997) 91–97.

[13] H. Beckers, P. Garcia, H. Willner, G.A. Argüello, C.J. Cobos, J.S. Francisco, Side-on versus end-on bonding of O_2 to the FSO_3 radical: matrix isolation and ab initio study of FSO_5, Ang. Chem. Int. Ed. 46 (2007) 3595–3605.

[14] E. Castellano, R. Gatti, J.E. Sicre, H.J. Schumacher, Das Gleichgewicht $F_2S_2O_6 \rightleftarrows 2\ FSO_3$, das Absorptionsspektrum des Radikals FSO_3 und die Kinetik der thermischen Reaktion zwischen Bis-Sulfurylfluoridperoxid und Schwefeltetrafluorid, Z. Phys. Chem. NF 42 (1964) 174–186.

[15] E. Castellano, H.J. Schumacher, La cinética de las reacciones térmicas del peróxido de bis-fluoro-sulfurilo con SO2 y con SF4. La energía de disociación DFSO3-SO2 y DFSO3-SF4 de los intermediarios FSO3-SO2 y FSO3-SF4, Anal. Asoc. Quím. Argentina. 55 (1967) 147–151.

[16] E. Castellano, H.J. Schumacher, Die Kinetik der thermischen reaction zwischen Bis-fluorosulfurylperoxid ($F_2S_2O_6$) und Schwefeldioxid, Z. Phys. Chem. NF 43 (1964) 66–70.

[17] J.E. Bolzan, J.E. Sicre, H.J. Schumacher, Die Bestimmung der Absolutgeschwindigkeit der Reaktionen zwischen F-Atomen und SO3-Molekülen bzw. FSO3-Radikalen, Z. Phys. Chem. NF 46 (1965) 78–87.

[18] F.B. Dudley, G.H. Cady, The equilibrium between peroxydisulfuryl difluoride and fluorosulfate free radicals, J. Am. Chem. Soc. 85 (1963) 3375–3377.

[19] P.M. Nutkowitz, G. Vincow, Electron spin resonance study of the $S_2O_6F_2$-SO_3F. equilibrium. Enthalpy of cleavage, J. Am. Chem. Soc. 91 (1969) 5956–5958.

[20] C.J. Cobos, A.E. Croce de Cobos, H. Hippler, E. Castellano, Direct determination of the limiting high pressure rate constants of the system $FSO_3 + FSO_3 \rightleftarrows F_2S_2O_6$ over the temperature range 293–381 K, J. Phys. Chem. 93 (1989) 3089–3094.

[21] R.A. de Marco, J.M. Shreeve, Fluorinated Peroxides, in: H.J. Emeléus, A.G. Sharpe (Ed.), Adv. Inorg. Chem and Radiochem, vol. 16, Academic Press, NY and London, 1974.

[22] E.C. Zimmermann, J. Ross, Light induced bistability in $S_2O_6F_2 \rightleftarrows 2\ SO_3F$: Theory and experiment, J. Chem. Phys. 80 (1984) 720–729.

[23] E.C. Zimmermann, M. Schell, J. Ross, Stabilization of unstable states and oscillatory phenomena in an illuminated thermochemical system: theory and experiment, J. Chem. Phys. 81 (1985) 1327–1336.

[24] J. Kamer, J. Reiter, J. Ross, Propagation of a chemical pulse in an illuminated thermochemical bistable system, J. Chem. Phys. 84 (1986) 1492–1499.

[25] E. Castellano, H.J. Schumacher, Die Kinetik der thermischen Reaktion zwischen Fluor und Bisfluorsulfurylperoxid, Z. Physik. Chem. NF 44 (1965) 44–66.

[26] W.H. Basualdo, H.J. Schumacher, Die photochemische Reaktionen von Fluorfluorsulfunat, F_2SO_3, mit Schwefeltrioxid und Schwefeldioxid im Licht der Wellenlänge 2537 Å, Z. Physik. Chem. NF 47 (1965) 57–64.

[27] R. Gatti, J.E. Sicre, H.J. Schumacher, Die Kinetik der thermischen Reaktion zwischen Bis-Fluorsulfurylperoxid, $F_2S_2O_6$, und Kohlenmonoxid, Z. Physik. Chem. NF 47 (1965) 323–336.

[28] R. Gatti, H.J. Schumacher, Die Kinetik der durch Bis-Fluorsulfurylperoxyd sensibilisierten Kohlendioxidbildung aus Kohlenmonoxid und Sauerstoff, Z. Physik. Chem. NF 55 (1967) 148–161.

[29] E. Vasini, H.J. Schumacher, Die Kinetik der thermischen Reaktion zwischen F_2SO_3 und CO, Z. Physik. Chem. NF 94 (1975) 39–52.

[30] G. von Ellenrieder, H.J. Schumacher, Die Kinetik der thermischen Zerfalles von Fluorfluorsulfonat in Gegenwart von Chlor, Z. Physik. Chem. NF 60 (1968) 49–57.

[31] E. Vasini, H.J. Schumacher, Die Kinetik der thermischen Reaktion zwischen Fluorfluorsulfonat, Kohlenmonoxid und Sauerstoff, Z. Physik. Chem. NF 104 (1977) 219–228.

[32] A.E. Croce de Cobos, C.J. Cobos, E. Castellano, Pressure and temperature dependence of the reaction $F + FSO_3 + M \rightarrow FSO_2OF + M$, J. Phys. Chem. 93 (1989) 274–278.

[33] A.E. Croce, C.J. Cobos, E. Castellano, Pulsed laser photolysis study of the reaction $Cl + FSO_3 + M \rightarrow FSO_2OCl + M$, Chem. Phys. Lett. 158 (1989) 157–160.

[34] C.J. Cobos, A.E. Croce, E. Castellano, Excimer laser-induced temperature jump-measurements on the recombination kinetics of the gas-phase $FSO_3 + FSO_3 \rightleftarrows F_2S_2O_6$ equilibrium between 415 and 525 K, Int. J. Chem. Kinet. 22 (1990) 289–297.

[35] M.E. Tucceri, M.P. Badenes, A.E. Croce, C.J. Cobos, Kinetics of formation of the novel peroxide $FC(O)OO(O_2)SF$, Chem. Comm. 71–72 (2001).

[36] M.E. Tucceri, M.P. Badenes, A.E. Croce, C.J. Cobos, Experimental and theoretical study of the recombination reaction of $FS(O_2)O$ with FC(O)O and CO, Phys. Chem. Chem. Phys. 3 (2001) 1832–1839.

[37] M.E. Tucceri, A.E. Croce, C.J. Cobos, Limiting high-pressure rate coefficient for the recombination reaction $FSO_2 + FSO_3 \rightarrow FS(O_2)O(O_2)SF$: An experimental and theoretical study, Chem. Phys. Lett. 404 (2005) 232–236.

[38] M.E. Tucceri, M.P. Badenes, A.E. Croce, C.J. Cobos, Experimental and theoretical study of the recombination reaction $FSO_2 + O_2 \rightarrow FS(O_2)OO$, Chem. Phys. Lett. 465 (2008) 15–19.

[39] G.W. King, D.P. Santry, C.H. Warren, The fluorosulfate radical: structural theory and assignment of electronic absorption systems, J. Mol. Spectrosc. 32 (1969) 108–120.

[40] G.W. King, C.H. Warren, The fluorosulfate radical: vibrational analysis of the 5160 Å absorption system, J. Mol. Spectrosc. 32 (1969) 121–137.

[41] G.W. King, C.H. Warren, The fluorosulfate radical: rotational analysis of the 5160 Å system and molecular geometry, J. Mol. Spectrosc. 32 (1969) 138–150.

[42] C.H. Warren, Resonance spectrum and production of the fluorosulfate radical by laser excitation, Chem. Phys. Lett. 53 (1978) 509–514.

[43] C.H. Warren, Laser fluorescence spectrum of the fluorosulfate radical 514.5 nm excitation, Chem. Phys. Lett. 68 (1979) 407–411.

[44] C.H. Warren, Argon-ion laser excitation of the fluorosulfate radical, J. Mol. Spectrosc. 83 (1980) 451–461.

[45] C.H. Warren, Dye laser excitation of the fluorosulfate radical: origin band excitation, J. Mol. Spectrosc. 84 (1980) 102–112.

[46] C.H. Warren, Dye laser excitation of the fluorosulfate radical. Totally symmetric upper state fundamentals, Chem. Phys. Lett. 72 (1980) 233–236.

[47] H. Beckers, H. Willner, D. Grote, W. Sander, EPR and IR spectra of the FSO_3 radical revisited: strong vibronic interactions in the $^2A_2$ electronic ground state, J. Chem. Phys. 128 (2008) 084501.

[48] L. Kolesniková, J. Varga, L.N. Striteská, H. Beckers, H. Willner, F. Aubke, S. Urban, The ground state rotational spectrum of the fluorosulfate radical, J. Chem. Phys. 130 (2009) 184309.

[49] G. Cady, J.E. Roberts, J. Am. Chem. Soc. 81 (1959) 4166.

[50] A.D. Becke, Density-functional exchange-energy approximation with correct asymptotic behavior, Phys. Rev. A 38 (1988) 3098–3100.

[51] C. Lee, W. Yang, R.G. Parr, Development of the Colle-Salvetti correlation-energy formula into a functional of the electron density, Phys. Rev. B 37 (1988) 785–789.

[52] H.L. Schmider, A.D. Becke, Optimized density functionals from the extended G2 test set, J. Chem. Phys. 108 (1998) 9624–9631.

[53] P.J. Wilson, T.J. Bradley, D.J. Tozer, Hybrid exchange-correlation functional determined from thermochemical data and ab initio potentials, J. Chem. Phys. 115 (2001) 9233–9242.

[54] C. Adamo, V. Barone, Exchange functionals with improved long-range behavior and adiabatic connection methods without adjustable parameters: the mPW and mPW1PW models, J. Chem. Phys. 108 (1998) 664–675.

[55] C. Adamo, V. Barone, Toward reliable density functional methods without adjustable parameters: the PBE0 model, J. Chem. Phys. 110 (1999) 6158–6169.

[56] A.J. Cohen, N.C. Handy, Dynamic correlation, Mol. Phys. 99 (2001) 607–615.

[57] X. Xu, W.A. Goddard III, The X3LYP extended density functional for accurate descriptions of nonbond interactions, spin states, and thermochemical properties, Proc. Natl. Acad. Sci. USA 101 (2004) 2673–2677.

[58] A.D. Boese, J.M.L. Martin, Development of density functionals for thermochemical kinetics, J. Chem. Phys. 121 (2004) 3405–3416.

[59] Y. Zhao, N.E. Schultz, D.G. Truhlar, Design of density functionals by combining the method of constraint satisfaction with parametrization for thermochemistry, thermochemical kinetics, and noncovalent interactions, J. Chem. Theory Comput. 2 (2006) 364–382.

[60] Y. Zhao, D.G. Truhlar, The M06 suite of density functionals for main group thermochemistry, thermochemical kinetics, noncovalent interactions, excited states, and transition elements: two new functionals and systematic testing of four M06-class functionals and 12 other functionals, Theor. Chem. Acc. 120 (2008) 215–241.

[61] Y. Zhao, D.G. Truhlar, Comparative DFT study of van der Waals complexes: rare-gas dimers, alkaline-earth dimers, zinc dimer, and zinc-rare-gas dimers, J. Phys. Chem. 110 (2006) 5121–5129.

[62] J.M. Tao, J.P. Perdew, V.N. Staroverov, G.E. Scuseria, Climbing the density functional ladder: nonempirical meta-generalized gradient approximation designed for molecules and solids, Phys. Rev. Lett. 91 (2003) 146401.

[63] A.D. Boese, N.C. Handy, New exchange–correlation density functionals: the role of the kinetic-energy density, J. Chem. Phys. 116 (2002) 9559–9569.

[64] M. Ernzerhof, J.P. Perdew, Generalized gradient approximation to the angle- and system-averaged exchange hole, J. Chem. Phys. 109 (1998) 3313–3320.

[65] O.A. Vydrov, G.E. Scuseria, Assessment of a long-range corrected hybrid functional, J. Chem. Phys. 125 (2006) 234109.

[66] T. Yanai, D. Tew, N. Handy, A new hybrid exchange-correlation functional using the Coulomb-attenuating method (CAM-B3LYP), Chem. Phys. Lett. 393 (2004) 51–57.

[67] J.-D. Chai, M. Head-Gordon, Long-range corrected hybrid density functionals with damped atom-atom dispersion corrections, Phys. Chem. Chem. Phys. 10 (2008) 6615–6620.

[68] A.V. Krukau, O.A. Vydrov, A.F. Izmaylov, G.E. Scuseria, Influence of the exchange screening parameter on the performance of screened hybrid functionals, J. Chem. Phys. 125 (2006) 224106.

[69] M.J. Frisch, J.A. Pople, J.S. Binkley, Self-consistent molecular orbital methods 25. Supplementry functions for Gaussian basis sets, J. Chem. Phys. 80 (1984) 3265–3269.

[70] J.A. Montgomery Jr., M.J. Frisch, J.W. Ochterski, G.A. Petersson, A complete basis set model chemistry. VI. Use of density functional geometries and frequencies, J. Chem. Phys. 110 (1999) 2822–2827.

[71] J.A. Montgomery Jr., M.J. Frisch, J.W. Ochterski, G.A. Petersson, A complete basis set model chemistry. VII. Use of the minimum population localization method, J. Chem. Phys. 112 (2000) 6532–6542.
[72] A.G. Baboul, L.A. Curtiss, P.C. Redfern, K. Raghavachari, Gaussian-3 theory using density functional geometries and zero-point energies, J. Chem. Phys. 110 (1999) 7650–7657.
[73] L.A. Curtiss, P.C. Redfern, K. Raghavachari, Gaussian-4 theory, J. Chem. Phys. 126 (2007) 084108.
[74] L.A. Curtiss, P.C. Redfern, K. Raghavachari, Gaussian-4 theory using reduced order perturbation theory, J. Chem. Phys. 127 (2007) 124105.
[75] B. Anantharaman, C.F. Melius, Bond additivity corrections for G3B3 and G3MP2B3 quantum chemistry methods, J. Phys. Chem. A 109 (2005) 1734–1747.
[76] M.P. Badenes, A.E. Croce, C.J. Cobos, Theoretical thermochemistry of the FSOx (x=1 to 5) radical series, in: A.G. Mirskiy (Ed.), Thermochemistry and Advances in Chemical Research, Nova Science Publishers Inc, New York, 2009, pp. 311–321.
[77] E. Runge, E.K.U. Gross, Density-functional theory for time-dependent systems, Phys. Rev. Lett. 52 (1984) 997–1000.
[78] M.J. Frisch, et al., Gaussian Inc., Revision A.02, Wallingford, CT, USA, 2009.
[79] S. Glasstone, K.J. Laidler, H. Eyring, The Theory of Rate Processes: The Kinetics of Chemical Reactions, Viscosity, Diffusion and Electrochemical Phenomena, McGraw-Hill Book Company Inc., New York, 1941.
[80] A.I. Maergoiz, E.E. Nikitin, J. Troe, V.G. Ushakov, Classical trajectory and statistical adiabatic channel study of the dynamics of capture and unimolecular bond fission. V. Valence interactions between two linear rotors, J. Chem. Phys. 108 (1998) 9987–9998.
[81] A.I. Maergoiz, E.E. Nikitin, J. Troe, V.G. Ushakov, Classical trajectory and statistical adiabatic channel study of the dynamics of capture and unimolecular bond fission. VI. Properties of transitional modes and specific rate constants k(E, J), J. Chem. Phys. 117 (2002) 4201–4213.
[82] W.J. Hehre, L. Radom, P. von R.Schleyer, J.A. Pople, Ab Initio Molecular Orbital Theory, Wiley, New York, 1986.
[83] S.W. Benson, Thermochemistry and kinetics of sulfur-containing molecules and radicals, Chem. Rev. 78 (1978) 23–35.
[84] K.B. Wiberg, R.E. Stratman, M.J. Frisch, A time-dependent density functional theory study of the electronically excited states of formaldehyde, acetaldehyde and acetone, Chem. Phys. Lett. 297 (1998) 60–64.
[85] S. Hirata, M. Head-Gordon, Time-dependent density functional theory for radicals. An improved description of excited states with substantial double excitation character, Chem. Phys. Lett. 302 (1999) 375–382.
[86] S.L. Manatt, A.L. Lane, A compiltion of the absorption cross-sections of SO_2 from 106 to 403 nm, J. Quant. Spectrosc. Radiat. Transfer 50 (1993) 267–276.
[87] J. Troe, Theory of thermal unimolecular reactions at low pressures. II. Strong collision rate constants. Applications, J. Chem. Phys. 66 (1977) 4758–4775.
[88] M.W. Chase, Jr., NIST-JANAF Thermochemical Tables, fourth ed., J. Phys. Chem. Ref. Data, 1988, Monograph No. 9.
[89] H.S.P. Müller, J. Farhoomand, E.A. Cohen, B. Brupbacher-Gatehouse, M. Schäfer, A. Bauder, G. Winnewisser, The rotational spectrum of SO_2 and the determination of the hyperfine constants and nuclear magnetic shielding tensors of $^{33}SO_2$ and $SO^{17}O$, J. Mol. Spectrosc. 201 (2000) 1–8.
[90] M. Quack, J. Troe, Specific rate constants of unimolecular processes. II. Adiabatic channel model, Ber. Bunsenges. Phys. Chem. 78 (1974) 240–252.
[91] C.J. Cobos, J. Troe, Theory of thermal unimolecular reactions at high pressures. II. Analysis of experimental results, J. Chem. Phys. 83 (1985) 1010–1015.
[92] C.J. Cobos, A.E. Croce, K. Luther, L. Soelter, E. Tellbach, Juergen Troe, Experimental and modeling study of the reaction C_2F_4 (+M) ⇄ CF_2 + CF_2 (+M), J. Phys. Chem. A 117 (2013) 11420–11429.
[93] A.E. Croce, C.J. Cobos, Theoretical kinetics study of the reactions forming the ClCO radical cycle in the middle atmosphere of Venus, Z. Phys. Chem. 229 (2015) 1541–1559.
[94] M.P. Badenes, M.E. Tucceri, C.J. Cobos, The role of the recombination channel in the reaction between the HO and HO_2 radicals, J. Phys. Chem. A 121 (2017) 440–447.